CHROMOSPHERIC EVAPORATION IN A TWO-RIBBON FLARE

G. Cauzzi[1], A. Falchi[1], L. Teriaca[1], R. Falciani[2], L.A. Smaldone[3], and V. Andretta[4]

[1]INAF-Osservatorio Astrofisico di Arcetri, Firenze, Italy
[2]Dipartimento di Astronomia e Scienza dello Spazio, Università di Firenze, Firenze, Italy
[3]Dipartimento di Scienze Fisiche, Università di Napoli "Federico II", 80126 Napoli, Italy
[4]INAF-Osservatorio Astronomico di Capodimonte, Napoli, Italy

ABSTRACT

We present simultaneous, spatially and temporally resolved chromospheric, transition region and coronal observations of a small eruptive flare studied throughout its whole development. We show that strong and co-spatial plasma motions, oppositely directed in the chromosphere (downflows) and in upper atmospheric layers (upflows), develop at the onset of the flare. For the first time, we prove that such oppositely directed flows originate from the same flaring kernels in different atmospheric layers. Using realistic values for the plasma parameters in the flaring loop, we also estimate a balance between the upward and downward momenta. Our observations confirm in a very convincing way the scenario of chromospheric evaporation predicted in theoretical models of flares.

Key words: Sun: activity; Sun: flares; Sun: atmospheric motions.

1. INTRODUCTION

Hydrodynamical models of flares stress the relevance of the so-called "explosive chromospheric evaporation", a sudden increase of the chromospheric temperature to coronal values, occurring when the chromospheric plasma is heated beyond its ability to radiate (Nagai & Emslie, 1984; Fisher, 1986; Gan et al., 1991). Chromospheric evaporation can explain the strong upward motions observed in coronal lines (up to 400 km s^{-1}, see e.g. Antonucci et al., 1982) and downward motions observed in the chromosphere (up to 100 km s^{-1}, see e.g. Ichimoto and Kurokawa, 1984), during the impulsive phase of a flare.

Given the common origin of the oppositely directed flows in the different atmospheric layers, the momenta of the downward and of the upward plasma should be balanced. Such a balance has been proven, within a factor of 2-6, only for a few events (Zarro et al., 1988, Canfield et al., 1990, Wülser et al., 1992), and always *assuming* that the locations of the blueshifted plasma and of the red shifted chromospheric material was the same, since the used spectral coronal observations were spatially unresolved.

The Coronal Diagnostic Spectrometer aboard SOHO (CDS, Harrison et al., 1995) is particularly suitable to address this topic, since it provides both spectral and spatial information with a good resolution. Using CDS, spatially resolved observations of blueshifts in transition region (TR) and coronal lines during the late gradual phase of a large two-ribbon flare have been obtained by Czaykowska et al. (1999). Similar observations of moderate upflows in low temperature coronal lines such as Mg X and Si XII during the development of a small flare have been presented by Del Zanna et al. (2002). In both cases, the authors interpreted such flows as evidence of chromospheric evaporation following the main flare energy release. However, it must be evidenced that *spatially resolved* and *simultaneous* observations of flows in chromospheric and upper atmospheric layers during the development of a flare are still lacking.

We contribute to this topic presenting here for the first time simultaneous, spatially and temporally resolved chromospheric, transition region and coronal observations of a small eruptive flare (GOES class C1.1), studied throughout its whole evolution. The flare developed in NOAA 9468 on May 26, 2001 around 16:00 UT ($\cos\theta$=0.99).

2. OBSERVATIONS

Data were acquired during SOHO JOP#139. Sequences of raster scans of the target Active Region were obtained in several TR and coronal lines by CDS, and in chromospheric lines by the Horizontal Spectrograph at the Dunn Solar Telescope (DST) of the NSO/Sacramento Peak.

CDS Data: The spectral lines observed with CDS-Normal Incidence Spectrometer were selected to

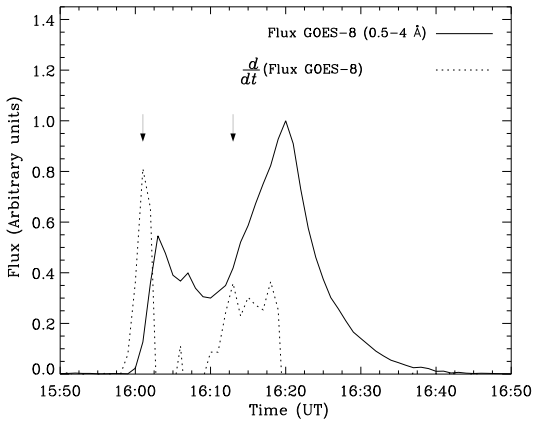

Figure 1. SXR full disk flux in the 0.5–4 Å band (solid line) and time derivative (dotted line) around the time of the flare (GOES-8 data). Local maxima in the derivative (∼ 16:01 and ∼ 16:13 UT) are marked by arrows.

cover a wide range of temperatures. We obtained raster scans in He I 584 (log T=4.3), He II 304 (log T=4.8), O V 630 (log T=5.4), Fe XVI 360 (log T=6.3), and Fe XIX 592 Å (log T=6.9). The final useful field of view (FOV) was $148'' \times 138''$, with a spatial resolution of $6'' \times 3.4''$/pixel. Temporal cadence was ∼ 14 s/slit position, and a full raster scan took about 5.5 min.

DST Data: Several chromospheric lines were monitored with the Horizontal Spectrograph at the DST: Ca II-K, Hα, He I 5876 Å (D3) and He I 10830 Å. We remark here that both these "chromospheric" He I lines are formed at lower layers than He I 584 Å. The final FOV was of $160'' \times 140''$, slightly shifted westward with respect to the CDS one. The spatial resolution was $2'' \times 2''$. Spectra at each slit position were recorded in 3.5 s, and a full raster scan of the AR took about 5 m. Finally, images within the Hα line were acquired on the same FOV by means of the Universal Birefringent Filter.

3. FLARE DEVELOPMENT

Figure 1 displays the GOES 0.5 - 4 Å soft X-ray flux around the time of the flare development. Since no hard X-ray (HXR) measurement was available, we used the time-derivative of the GOES flux as a proxy for the HXR emission (Neupert effect. See Dennis & Zarro, 1993, and Veronig et al., 2002, for a discussion on such an assumption). Two main bursts in the derivative are visible at ∼ 16:01 and ∼ 16:13 UT, with the first one much more abrupt and intense than the second one, although the global SXR emission peaks only at 16:20 UT.

The general flare development is depicted in Figure 2. The dashed white line in panel *c* indicates the magnetic neutral line derived from a MDI full disk magnetogram. Although quite small, the flare displays all the characteristics of an eruptive event: strong upward chromospheric motions (see Sec. 4) betray the eruption of the thin AR filament visible in panel *a*; two flaring ribbons with evidence of ongoing magnetic reconnection develop afterwards (panels *b* and *c*); a long decay phase (panel *d*) last more than 40 minutes from the second soft X-ray peak, with new flaring kernels developing further away form the neutral line.

The intensity evolution during the flare can be summarized as follows (a relevant figure can be found in Teriaca et al., 2002):

The strongest emission in TR lines (O V, He I 584, He II 304 Å) occurs during the early phase of the flare, and pertains to small and very localized kernels spatially coincident with the chromospheric flaring footpoints. Maximum radiance values are about 60 (in O V) and 10-15 times (in He I and He II lines) the pre-flare radiance. The emission in TR lines has a very impulsive behavior, but still outlines well the chromospheric flaring areas even during secondary episodes of energy release, such as those producing the new flaring kernels around the time of the second "Neupert peak". This is consistent with earlier results presented by, e.g., Woodgate et al. (1983), Cheng (1984), Cheng et al. (1988).

Coronal emission as measured in Fe XVI and Fe XIX is instead mostly located between the ribbons, and peaks well after the TR emission. Maximum radiance values for Fe XVI are of the order of 4 times the pre-flare ones, while Fe XIX (indicating plasma at 7-8 MK) is not present before the flare. This seems to validate the idea that the flare energy is released impulsively in the corona and transported by accelerated non-thermal electrons or by thermal conduction to the loop footpoints. The heated chromospheric material then flows up into the loop and produces the gradually rising soft X-ray signal (e.g, Hudson & Ryan, 1995).

4. VELOCITY EVOLUTION

The AR filament visible in the pre-flare Hα images (Fig. 2 *a*) becomes destabilized and erupts slightly earlier than the first Neupert peak. The eruption is clearly measured as upwards motions of 10-20 km s^{-1} in the chromospheric lines around ∼16:00:30 UT, as displayed in Figure 3 *a*. No flows in these positions are measured in the TR or coronal data.

Strong downflows (30-40 km s^{-1}) following the shape of the developing ribbons are measured in He I 10830 in the successive raster scan (around 16:05 UT; Fig. 3 *b*). Note that the location of intense chromospheric downflows is quite different than the one of previous upflows. In panel *b*, it is also shown that cospatial and quasi simultaneous (16:02:30 UT) strong upward motions are instead measured in O V, with values reaching −100 km s^{-1}. Measures of flows in

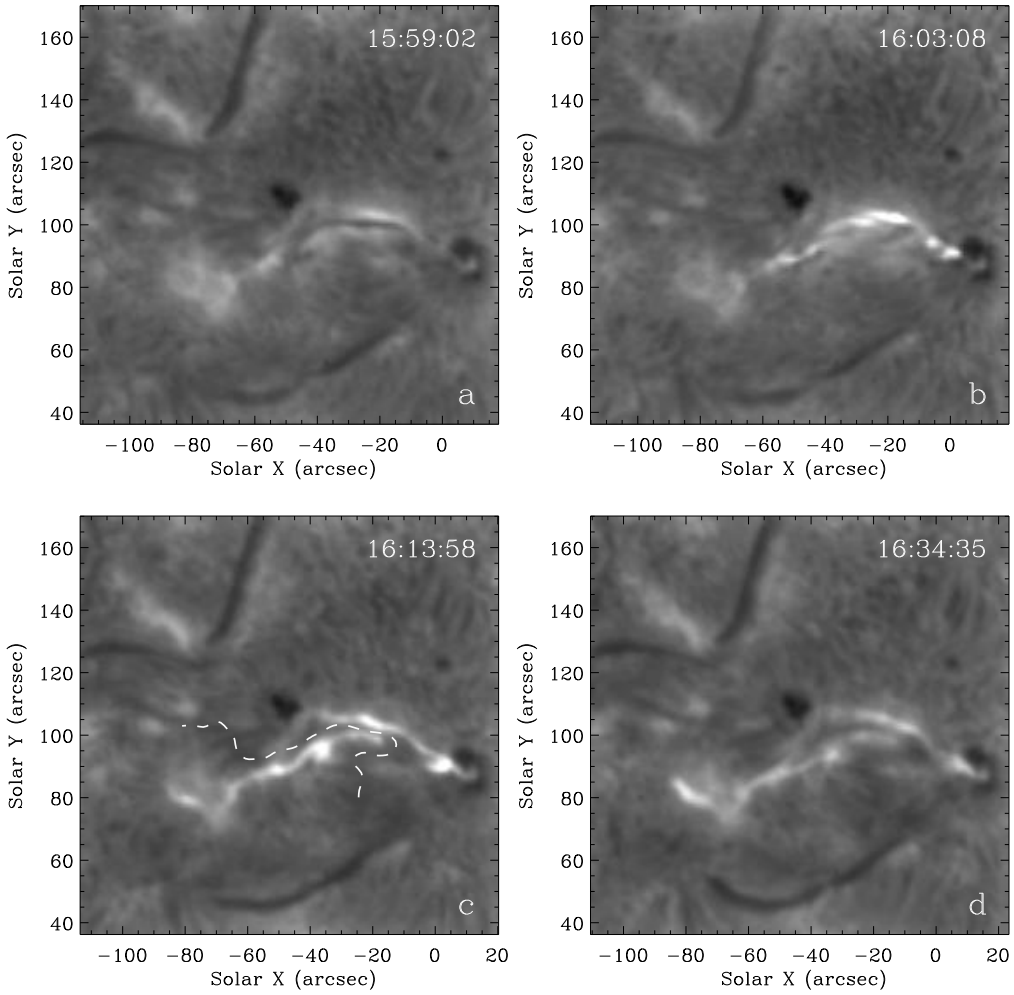

Figure 2. UBF Hα images summarizing the flare evolution. X direction is parallel to the solar equator. Image scale is the same for all panels. (a) Pre-flare phase. At this time, the filament within the active region is thickening and undergoing upward motions. (b) First phase of ribbon development. (c) Second major energy release episode. The dashed line represents the magnetic inversion line. (d) Decay phase. New, less intense kernels develop further away from the neutral line.

He I 584 provide the same spatial pattern of upward velocities, although with values a factor two lower. Finally, upflows of about -150 km s^{-1} are also measured with the Fe XIX 592 coronal line at this time, over the area of maximum O V velocities. Although similar upflows in the TR and corona during a flare development had been presented by other authors (Czaykowska et al., 1999; Del Zanna et al., 2002), this is the *first time* that quasi-simultaneous and opposite directed motions in different atmospheric layers are observed in the same spatial location during a flare.

5. MOMENTUM BALANCE

Following the arguments given in the Introduction, we compared the *instantaneous momenta* of the downward moving chromospheric plasma (∼16:05 UT) with that of the upward moving coronal plasma (∼16:02:30 UT). The underlying assumption is that these flows, although not exactly simultaneous, are representative of typical "flaring episodes".

Downflow momentum in the chromosphere can be written as:

$$P_{down} = \mu m_H n_{ch} A v_{ch} \Delta h$$

with μ (mean atomic mass) = 1.56. n_{ch} is the *preflare* chromospheric density, A is the area interested by flows, and Δh represents the thickness of the chromospheric condensation. Using n_{ch} and Δh values derived from semi-empirical models of the preflare atmosphere (Mauas 2002, private communication), we obtain:

$$1.2 \times 10^{19} \text{ gr cm s}^{-1} \leq P_{down} \leq 1.2 \times 10^{20} \text{ gr cm s}^{-1}$$

At coronal level, the momentum of the upflowing plasma is given by:

$$P_{up} = \mu m_H \sqrt{EM_L \; S^2 \; L} \; v_{cor}$$

where S is the area of the region from where

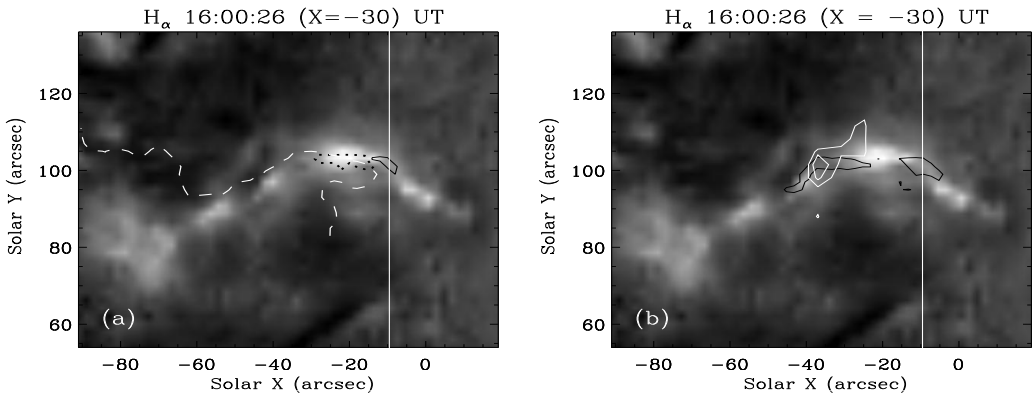

Figure 3. (a): Velocity contours for chromospheric He I *10830 around 16:00:26 UT (-20 km s^{-1} – black dotted lines and 20 km s^{-1} – black solid lines. Upward is negative). The background H$_\alpha$ image is simultaneous to the He* I *10830 measurements. The blueshifted pattern betrays the filament eruption before the flare. (b): Contours of He* I *10830 downflows measured around 16:05:14 UT (+25 km s^{-1}, black solid lines), overlaid on the same image of panel a. Isocontours of the velocities measured around 16:02:30 UT with the O* V *630 (-80, -60 km s^{-1} – white solid line) are also shown. The thin straight line indicates the limit of CDS FOV.*

blueshifted profiles arise, L the thickness of the emitting region, v_{cor} the plasma speed at coronal level, and EM_L the column emission measure. Assuming $L = \sqrt{S}$, and $v_{cor} \sim 150$ km s^{-1} , we obtain:

$$P_{up} = 6.5 \times 10^{19} \text{ gr cm s}^{-1}$$

In the assumption of a single flaring loop the contribution of TR plasma to the total upward momentum is negligible, given the very small thickness of the TR. Hence, given the uncertainties, especially in the determination of the volume involved, and the possible departures from ionization equilibrium in the flaring corona, the value of P_{up} evaluated for the corona well agrees with the P_{down} calculated in the chromosphere.

6. CONCLUSIONS

We presented here for the first time quasi-simultaneous, spatially and temporally resolved chromospheric, transition region and coronal observations of a small eruptive flare, studied throughout its whole development. Such a complete dataset allowed us to properly test the model of chromospheric evaporation, by means of a comparison between location, timing, amplitude and direction of the plasma motions developing during the flare in different atmospheric layers.

We show that strong and co-spatial plasma motions, oppositely directed in the chromosphere (downflows, up to ~ 40 km s^{-1}) and in upper atmospheric layers (upflows, up to ~ -150 km s^{-1}), develop at the onset of the flare. We prove for the first time that such oppositely directed flows originate from the same flaring kernels in different atmospheric layers.

Using plasma parameters derived from semi-empirical models of the pre-flare atmosphere, we found a balance between the "instantaneous" upward coronal and downward chromospheric momenta within a factor of 2–5. This seems to nicely confirm the scenario of chromospheric evaporation predicted in theoretical models of flares.

REFERENCES

Antonucci, E., et al., 1982, Solar Phys., 78, 107

Canfield, R. C., Zarro, D. M., Metcalf, T. R., & Lemen, J. R. 1990, ApJ, 348, 333

Cheng, C. C., 1984, Mem. S.A.It., 55, 663

Cheng, C. C, Vanderveen, K., Orwig, L. E., & Tandberg-Hanssen, E., 1988, ApJ, 330, 480.

Czaykowska, A., de Pontieu, B., Alexander, D., & Rank, G. 1999, ApJ, 521, L75

Del Zanna, G., et al., 2002, Adv. Space Res., Vol. 30, No. 3, 551

Dennis, B., & Zarro, D. M. 1993, Solar Phys., 146, 177

Fisher, G. H., 1986, Lecture Notes in Phys., 255, 53

Gan, W. Q., Zhang, H. Q., & Fang, C. 1991, A&A, 241, 618

Harrison R. A., et al. 1995, Solar Phys., 162, 233

Hudson, H., & Ryan, J. 1995, ARA&A, 33, 239

Ichimoto K., & Kurokawa K., 1984, Solar Phys., 93, 105

Nagai, F., & Emslie, A. G., 1984, ApJ, 279, 896

Teriaca, L., et al., 2002, ESA SP Series (SP-508), 457, A. Wilson ed.

Veronig, A., et al., 2002, A&A, 392, 699

Woodgate, B. E., Shine, R. A., Poland, A. I., & Orwig, L. E. 1983, ApJ, 265, 530

Wülser, J. P., Zarro, D. M., & Canfield, R. C. 1992, ApJ, 384, 341

Zarro D. M., Canfield R. C., Strong K. T., & Metcalf T. R. 1988, ApJ, 324, 582